Preliminary investigation on the melting behavior of a freeze-valve for the Molten Salt Fast Reactor

Tiberga, Marco; Shafer, Devaja; Lathouwers, Danny; Rohde, Martin; Kloosterman, Jan Leen

DOI
10.1016/j.anucene.2019.06.039

Publication date
2019

Document Version
Final published version

Published in
Annals of Nuclear Energy

Annals of Nuclear Energy 132 (2019) 544–554

Contents lists available at ScienceDirect

Annals of Nuclear Energy

journal homepage: www.elsevier.com/locate/anucene

Preliminary investigation on the melting behavior of a freeze-valve for the Molten Salt Fast Reactor

Marco Tiberga *, Devaja Shafer, Danny Lathouwers, Martin Rohde, Jan Leen Kloosterman

Technical University of Delft, Department of Radiation Science and Technology, Mekelweg 15, 2629 JB Delft, The Netherlands

ARTICLE INFO

Article history:
Received 30 January 2019
Received in revised form 16 June 2019
Accepted 19 June 2019

Keywords:
Freeze-plug
Passive safety device
Molten Salt Fast Reactor
Melting simulation
Apparent heat capacity method
Design improvement

ABSTRACT

This paper focuses on the freeze-plug, a key safety component of the Molten Salt Fast Reactor, one of the Gen. IV nuclear reactors that must excel in safety, reliability, and sustainability. The freeze-plug is a valve made of frozen fuel salt, designed to melt when an event requiring the core drainage occurs. Melting and draining must be passive, relying on decay heat and gravity, and must occur before the reactor incurs structural damage. In this work, we preliminarily investigate the freeze-plug melting behavior, assessing the influence of various design configurations and parameters (e.g., sub-cooling, recess depth). We used COMSOL Multiphysics® to simulate melting, adopting an apparent heat capacity method. Results show that single-plug designs generally outperform multi-plug ones, where melting is inhibited by the formation of a frozen layer on top of the metal grate hosting the plugs. The layer thickness strongly depends on sub-cooling and recess depth. For multi-plug designs, the P/D ratio has a negligible influence on melting and can therefore be chosen to optimize the draining time. The absence of significant mixing in the pipe region above the plug leads to acceptable melting times (i.e., <1000 s) only for distances from the core up to 0.1 m, considered insufficient to host all the cooling equipment on the outside of the draining pipe and to protect the plug from possible large temperature oscillations in the core. Consequently, we conclude that the current freeze-plug design based only on decay heat to melt is likely to be unfeasible. A design improvement, preserving passivity and studied within the SAMOFAR project (http://samofar.eu/), consists in accelerating melting via heat stored in steel masses adjacent to the draining pipe.

1. Introduction

First conceived during the post-World War II era to propel strategic bombers, molten salt reactors were then investigated for civilian purposes at Oak Ridge National Lab (ORNL) in the late fifties and sixties (MacPherson, 1985). The program led to the development and the construction of the Molten Salt Reactor Experiment (MSRE), a 7.5 MW_{th} test reactor that successfully operated from 1965 to 1969, demonstrating the safety and the feasibility of the technology (Haubenreich and Engel, 1970). However, the program was shutdown in 1970 and the US government funds ceased, in favor of sodium cooled reactor research.

Over the past two decades, interest in MSR technology regained momentum (LeBlanc, 2010), especially after the Molten Salt Fast Reactor (MSFR) was selected as one of the six Generation IV nuclear reactors (Generation IV International Forum, 2002). These reactors must excel in safety, reliability, and sustainability, to help meet the world's rising energy needs, while accommodating the concerns about waste storage, proliferation, and safety grown in a large part of the public and political parties, especially following the Fukushima Daichi accident. The H2020 Euratom SAMOFAR project (http://samofar.eu/) is currently coordinating the research efforts on the MSFR; its main goal is to prove the safety and the reliability of the current reactor design, or, on the other hand, to identify weak points to be further improved.

The current MSFR concept (Serp et al., 2014; Gérardin et al., 2017) is a fast-spectrum, 3000 MW_{th}, breeder reactor operating in the thorium fuel cycle. The liquid fuel and coolant is a mixture of lithium, thorium, and uranium fluorides; due to the high boiling point (around 1800 °C), this salt allows for operations at ambient pressure, and it is characterized by a strong negative temperature feedback coefficient (Heuer et al., 2014). This increases the safety of the design and lowers construction costs. Moreover, the fast spectrum, the daily fuel treatment (continuous on-line gas bubbling and delayed on-site reprocessing in batches of a few liters per day (Allibert et al., 2016)), and the salt recirculation lead to high burnup and actinides burning, and, thus, to low radiotoxicity, less actinide waste, and better fuel utilization (LeBlanc, 2010). Fig. 1 shows a schematic cross section of the MSFR primary circuit.

* Corresponding author.
E-mail address: M.Tiberga@tudelft.nl (M. Tiberga).

https://doi.org/10.1016/j.anucene.2019.06.039
0306-4549/

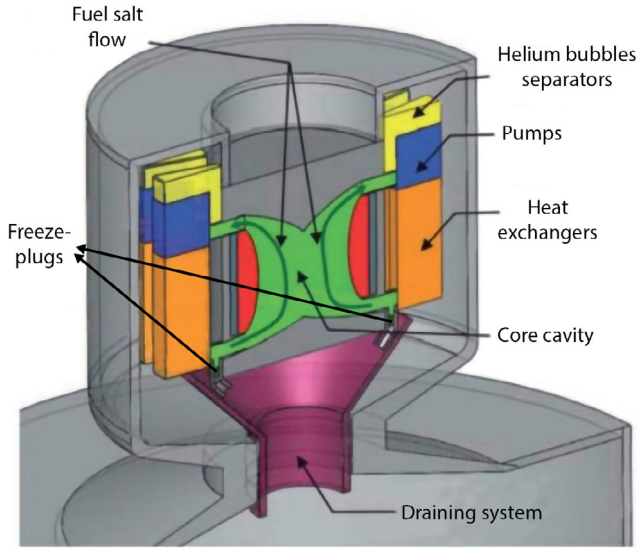

Fig. 1. Schematic view of the MSFR fuel circuit and draining system.

The salt rises in the core cavity and flows out towards sixteen identical sectors, each containing a helium bubble separation system, a pump, a heat exchanger, and a helium injection unit (not shown). The core cavity is surrounded by a toroidal blanket, where breeding takes place. Axial and radial reflectors are also present to improve the neutron economy and increase the breeding ratio.

This paper focuses on a key safety component of the MSFR: the freeze-plug. It is a valve made of frozen fuel salt, designed to melt in case of an event requiring the drainage of the core, like heat exchangers failure or power outage. During these accidents, in absence of a fully functioning heat sink, the decay heat released by fission products causes a temperature rise in the core that could eventually compromise the reactor's structural integrity. When the plug melts, on the other hand, the liquid salt is drained by gravity into a tank placed underneath the core, where it is safely cooled down without return to criticality thanks to the geometry of the tank.

The freeze-plug valve was first developed at ORNL and used during the MSRE (Richardson, 1962; Robertson, 1965). Formed by first pumping the salt into the core by pressure difference and then applying a cooling gas flow to the outside of the draining pipe, the plug was designed to melt when the cooling supply was turned off, by either exploiting the residual heat in the pipe or turning on external heaters. The valve was horizontal and was formed in a flattened section of pipe with dimensions $2.0 \times 6.3 \times 5.0$ cm and was capable of thawing in 5 min with the use of the external heater, and in less than 10 min passively.

The Shanghai Institute of Applied Physics developed a freeze-valve design close to the ORNL one for the Chinese Thorium MSR concept (Jiang et al., 2012), installing and successfully employing a prototype in a high temperature fluoride salt test loop (Kong et al., 2018). Aji et al. (2018) recently published results on preliminary experimental activities carried out to understand the influence of design parameters like plug dimensions and wall thickness on melting time.

A freeze-valve was installed as a safety device also in the Forced Fluoride Flow for Experimental Research (FFFER) loop built at LPSC-Grenoble (CNRS, France) laboratories (Giraud et al., 2018). The main goal of this facility is to study the liquid-gas separation to be exploited for the on-line cleaning of the molten salt, but tests were carried out to study the plug's formation and opening, helping improve the valve design. As the MSRE concept, the freeze valve is horizontal and its operational mode is controlled with heaters and coolers; however, contrarily to the MSRE valve, steel masses are used to store heat during nominal operations and speed up (passive) plug melting in case of total loss of power to the loop.

The current reference MSFR configuration includes a vertical freeze-plug at the base of each of the sixteen sectors of the primary circuit (Fig. 1). The plugs are based on the ORNL design, but must melt passively, relying only on the transfer of decay heat from the core cavity to the plug, mainly through the draining pipe walls, to melt. Within SAMOFAR, several numerical and experimental activities are currently ongoing to accurately study the solidification/melting processes governing the functioning of the freeze-plug (Rubiolo et al., 2017; Tano Retamales et al., 2017; Rubiolo et al., 2018; Giraud et al., 2018).

This work aims at preliminarily investigating, via numerical simulations, the melting behavior of the freeze-plug valve, as currently conceived for the reference MSFR concept, during a power outage accident followed by reactor shutdown. This is considered the most severe accident in which the freeze-plug valve has to prove its reliability. In fact, other accidents imply the availability of electricity, so other active valves can be used to drain the salt if needed. The influence of various design configurations and parameters, such as the plug position along the draining pipe and the sub-cooling at nominal conditions is assessed. Melting simulations were run adopting an apparent heat capacity method within the Finite Element tool COMSOL Multiphysics® (2017). Since only few design parameters are currently set for the freeze-plug, the conclusions drawn here could guide the future development of the component.

The remainder of the paper is organized as follows. In Section 2, the freeze-plug design is described, together with the parameters varied in the assessment. In Section 3, the modeling approach is presented: we introduce the melting problem and provide some details on the COMSOL simulations and the assumptions behind them. The results of the simulations performed for the different plug designs are presented in Section 4. Finally, in Section 5, we draw some conclusions, together with some recommendations for future studies on the freeze-plug valve.

2. Design under study

Fig. 2 shows vertical cross sections of the freeze-plug designs considered in this work: a single plug, occupying the full width of the draining pipe, along with a design consisting of 7 smaller plugs in a copper plate (see also Fig. 3b, for the top view of the latter). The latter design is based on the principle that having multiple plugs inside a plate accelerates melting due to the higher contact surface with the plate with respect to plug volume. The idea was originally proposed by Kloosterman and Rohde (Van Tuyll, 2016) and further investigated in Makkinje (2017). Even though the results in those studies were very preliminary and not fully error-free, the main design idea is considered promising and therefore further analyzed in this work.

The freeze-valve has to melt before the structural materials reach a temperature of 1200 °C, to avoid structural damage (Brovchenko et al., 2013); however, there is no definitive estimate for how long this will take: between 480 s (Brovchenko et al., 2013) and 1340 s (Tano Retamales et al., 2018). For this reason, an intermediate melting time threshold of 1000 s was considered throughout the assessment.

Table 1 shows the design parameters varied in this study. The ratio of pitch (P, i.e., the distance between the centers of two adjacent plugs, see Fig. 3b) to diameter (D) and the amount of sub-cooling (ΔT_{sub}, defined as the difference between the salt melting temperature and the cooling device temperature, which, as

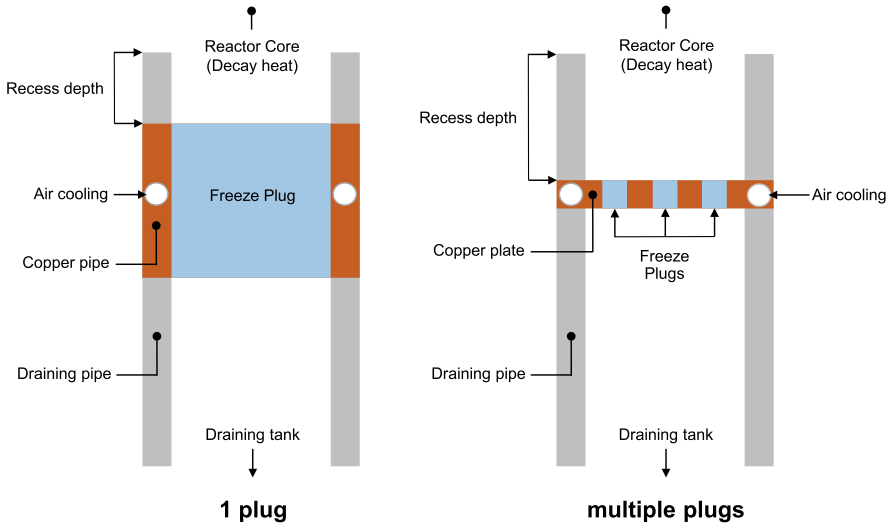

Fig. 2. Vertical cross sections of the freeze-plug designs featuring both one-plug and multiple-plug configurations.

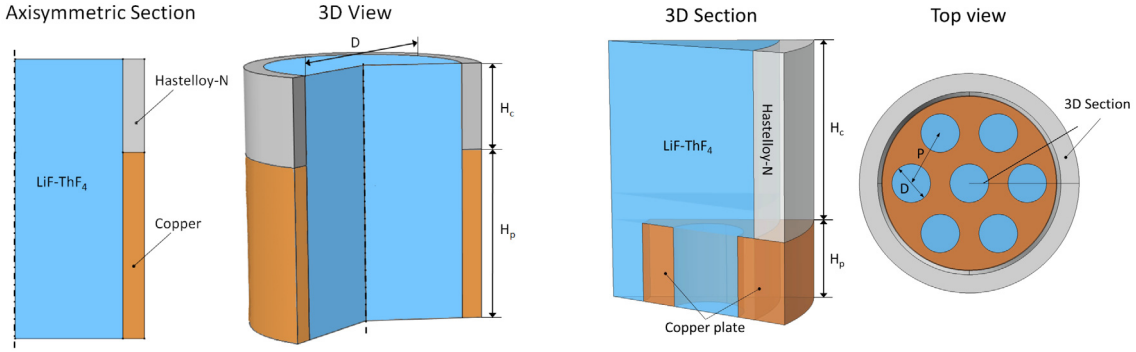

(a) Geometry and materials of the 1-plug design.

(b) Geometry and materials of the 7-plugs design.

Fig. 3. Geometries and materials used for the simulations of the 1-plug (left) and the 7-plugs (right) designs. D is the plug diameter, P the pitch, H_c the recess depth, H_p the height of the copper pipe section or of the plate hosting the multiple plugs.

Table 1
Freeze-plug parameters varied in this study for both the single and the multi-plug designs.

Parameter	Values considered
Recess depth, H_c (m)	0.01, 0.05, 0.1, 0.15, 0.2
P/D ratio	1.05, 1.25, 1.5
Sub-cooling, ΔT_{sub} (K)	5, 10, 15, 20, 25

explained in Section 3.2, can be considered equal to the minimum temperature in the plug) were investigated due to their influence on the steady-state shape of the freeze-plug; moreover, the latter increases the energy required to melt the plug. The actual sub-cooling is an unknown parameter, so we chose a range with reasonable extremes. In fact, keeping ΔT_{sub} too small increases the possibility of the plug melting prematurely, for example due to variability in the cooling power, or core temperature. On the other hand, a too large ΔT_{sub} slows down the melting process substantially.

After loss of power and subsequent reactor shutdown, the mean velocity in the core is expected to decrease rapidly (Tano Retamales et al., 2018); this, together with the salt temperature rise, leads to a fast increase of the bulk Richardson number, which suppresses mixing of decay heat in the cavity above the plug

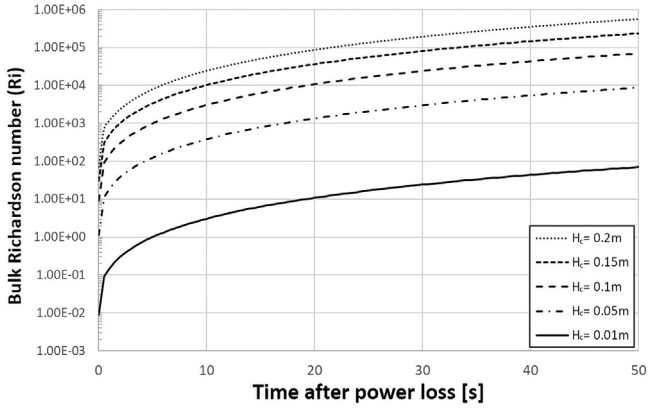

Fig. 4. Trend of salt bulk Richardson number after loss of power for increasing distance of the freeze-plug from the core cavity. The increase quickly suppresses heat transfer by convection.

(Iwatsu et al., 1993). Fig. 4 shows the expected time trend of the Richardson number, estimated from the trends of the mean salt temperature and velocity in the core after shutdown. Due to the increase of the Richardson number, heat transfer to the freeze-plug is dominated by conduction after loss of power. For this

reason, convection was not accounted for in this work, as well as radiative heat transfer, due to the absence of information on the salt optical properties in literature at the time of this study; this significantly reduces the computational effort and is a conservative approximation. Therefore, the distance of the plug from the core cavity (H_c, see Fig. 3b), concisely indicated with "recess depth" throughout this work, is a relevant parameter because it strongly affects the total heat flux reaching the plug.

The reference salt used in all simulations is LiF-ThF_4 (Beneš and Konings, 2009), at eutectic composition. The draining pipe above the plug was assumed made of Hastelloy-N, due to its compatibility with the salt (i.e., low corrosion rates) (Koger, 1972), while the pipe adjacent to the freeze-plug (or the plate holding the multiple plugs) made of copper (Fig. 3), due to its high thermal conductivity and relatively small specific heat capacity. The low melting temperature of copper (1085 °C) makes it unsuitable for a realistic configuration, where it has to be replaced by an alloy (not yet defined at the time of this study) which can withstand salt contact and high temperatures. Defining a fully realistic design lies outside the goal of the present analysis, but the results reported and the conclusions drawn here are valid provided that the material chosen for the realistic design has a thermal diffusivity closer to that of copper ($\approx 1.2 \cdot 10^{-4}$ $m^2 s^{-1}$) than to that of salt ($\approx 4.1 \cdot 10^{-7}$ $m^2 s^{-1}$). In this way, in fact, the dominant resistance of the heat transfer in the melting process remains at the interface between the salt and the plate.

Table 2 summarizes the material properties used during this assessment. Note that the solid LiF-ThF_4 properties are given for 816 K and calculated by a weighted average based on molar mass percentage; moreover, given the absence of data on the thermal conductivity for the solid phase, it was supposed to be equal to the liquid one. Following previous studies on reactor draining (Wang et al., 2016), the pipe inner diameter was set at 0.2 m, while the wall thickness of the draining pipe was kept constant at 0.02 m.

The size of the freeze-plugs in the multi-plug configuration was determined from circle-packing theory, which defines the maximum diameter (D_{max}) of a hole packed in a circle of radius R (e.g., Friedman, 2005; Graham, 1968). For seven holes, $D_{max} = 2R/3$. This is clearly equivalent to the pitch P. The actual plug diameter is smaller than D_{max}, because it is necessary to maintain some copper between the individual plugs for the structural integrity of the copper grate and in order to conduct heat to the sides of the plugs. Imposing a certain P/D ratio, one can easily derive the plug diameter from $D = (P/D)^{-1} D_{max}$. In all designs, the height of the copper plate (or pipe portion) in contact with the salt (H_p, see Fig. 3) was considered equal to the plug diameter, to guarantee an aspect ratio of one.

3. Modelling approach

3.1. Melting problem and apparent heat capacity method

Since the plug is made of salt at eutectic composition, the melting process is characterized by sharp phase-change fronts, where the material remains at the melting temperature (T_m) until it has absorbed sufficient energy to overcome the binding forces that maintain its solid structure, that is, the latent heat (L_H) (Alexiades and Solomon, 1993). The process can be described by the following set of partial differential equations, supposing constant properties in each phase (Nikrityuk, 2011):

$$\frac{\partial T_l(\mathbf{x},t)}{\partial t} = \alpha_l \nabla^2 T_l(\mathbf{x},t); \tag{1}$$

$$\frac{\partial T_s(\mathbf{x},t)}{\partial t} = \alpha_s \nabla^2 T_s(\mathbf{x},t); \tag{2}$$

$$k_s \nabla T_s(\mathbf{x},t) - k_l \nabla T_l(\mathbf{x},t) = L_H \rho_s \frac{\mathrm{d}s(t)}{\mathrm{d}t}. \tag{3}$$

Here, T is the temperature, α the thermal diffusivity, k the thermal conductivity, and ρ the density. The subscripts s and l indicate the solid and liquid phases, respectively. Besides the standard heat diffusion equation for both solid and liquid phases (Eqs. (1) and (2)), the additional Stefan condition (3) is required to describe the unknown location of the phase-change interface (s); it relates the melting front normal velocity ($\mathrm{d}s/\mathrm{d}t$), to the difference in heat flux across the front itself.

In this work, the melting process was simulated adopting the widely used apparent heat capacity method, available in the Finite Element tool COMSOL Multiphysics® (2017). This method involves reformulating the heat equation to account for the enthalpy jump at the phase-change interface (Voller et al., 1990; Swaminathan and Voller, 1993). The phase of the material undergoing phase-change is no longer represented by a step function from solid to liquid at the melting interface, but it is smeared over a "mushy zone" defined by the interval $2\Delta T$ around the melting temperature. In this region, the liquid fraction is assumed to be a linear function of the temperature as shown in Fig. 5, and according to Eq. (4).

$$\theta_l = \begin{cases} 1 & T > T_m + \Delta T; \\ \frac{(T - T_m + \Delta T)}{2\Delta T} & T_m - \Delta T < T < T_m + \Delta T; \\ 0 & T_m - \Delta T \geqslant T. \end{cases} \tag{4}$$

In the apparent heat capacity method, the Stefan condition (3) does not have to be solved for explicitly, because the melting front is implicitly tracked by taking into account the latent heat through a modified specific heat capacity term, c_{app}:

$$c_{app} = \begin{cases} c_{pl} & T > T_m + \Delta T; \\ \frac{1}{\rho}(\theta_l \rho_l c_{pl} + \theta_s \rho_s c_{ps}) + L_H \frac{d\xi_m}{dT} & T_m - \Delta T < T < T_m + \Delta T; \\ c_{ps} & T_m - \Delta T \geqslant T, \end{cases} \tag{5}$$

where θ_s is the solid phase-change indicator, defined as $\theta_s = 1 - \theta_l$, and ξ_m is the mass fraction, defined as

$$\xi_m = \frac{1}{2} \frac{\theta_l \rho_l - \theta_s \rho_s}{\rho}. \tag{6}$$

The density is defined in terms of the liquid and solid phase fractions as

Table 2
Relevant material properties used in this study.

Property	LiF-ThF_4[a]		Hastelloy-N	Copper
	Solid	Liquid		
Thermal conductivity (W m^{-1} K^{-1})	1.5	1.5	23.6	401
Density (kg m^{-3})	4502	4390	8860	8960
Specific heat capacity (J kg^{-1} K^{-1})	815	1000	578	377
Latent heat (J kg^{-1})	$1.59 \cdot 10^5$[b]		–	–
Melting temperature, T_m (K)	841		–	–

[a] Beneš and Konings (2009).
[b] Capelli et al. (2013).

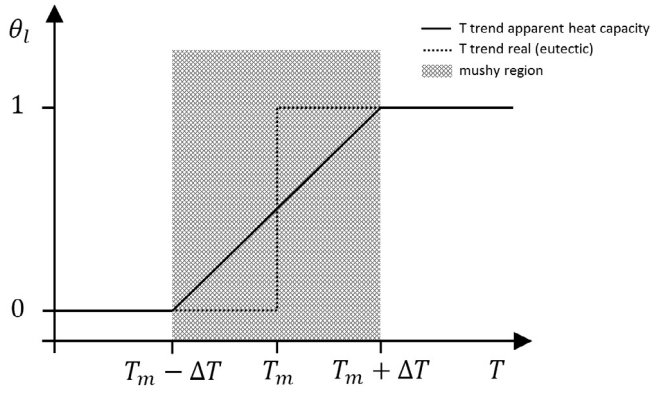

Fig. 5. Schematic representation of the approximation of sharp melting fronts into a mushy region which the apparent heat capacity method is founded on.

$$\rho = \theta_s \rho_s + \theta_l \rho_l. \tag{7}$$

The method got popular because of its versatility and convenience: it is easy to adapt to complex geometries and to implement, since the system (1)–(3) can be recast into a single diffusion equation (Jin et al., 2018):

$$\rho c_{app} \frac{\partial T(\mathbf{x}, t)}{\partial t} = k \nabla^2 T(\mathbf{x}, t), \tag{8}$$

where

$$k = \theta_s k_s + \theta_l k_l. \tag{9}$$

Accuracy. The accuracy of the apparent heat capacity method depends on the mesh and the computational time step sizes, and on the phase-change temperature range (ΔT) (Voller and Cross, 1981; Jin et al., 2018). With implicit discretization of the heat equation, the non-linearity is solved by taking the apparent heat capacity from the previous time step to compute the temperature at a certain node, which leads to calculation errors whenever a cell undergoes phase-change. For example, if the temperature at a node increases from the solid phase to the mushy zone within one time step, the apparent heat capacity from the solid phase is used to compute the temperature, and this leads to an exaggerated temperature increase, since no latent heat is accounted for. More serious errors occur if the temperature at a node increases from below $T_m - \Delta T$ to above $T_m + \Delta T$ in one time step, because the latent heat absorption and associated phase-change process is not taken into account at all. To avoid this, Voller and Cross (1981) recommend to choose the mesh size and time step such that at least two nodal temperatures lie within the phase-change range at each time step.

Moreover, Jin et al. (2018) found that the magnitude of ΔT relative to the amount of heating applied to the phase-change material strongly affects the error magnitude; if ΔT is chosen too large, the mushy zone could cover the entire solid phase, such that the liquid fraction throughout the entire solid phase is greater than zero. This would mean that the latent heat is not fully accounted for within the apparent heat capacity term, causing accelerated melting, particularly for eutectic or pure materials which in reality have sharp melting fronts. As a general rule of thumb, ΔT should be chosen smaller than the sub-cooling (COMSOL Multiphysics®, 2017).

3.2. COMSOL model and implementation

As shown in Figs. 3 and 6, a 2D, axisymmetric model was adopted for the single plug design, while a 3D wedge of 30°, with symmetry boundary conditions on the interior surfaces, was used as domain for the 7-plug design. The choice of the two different models is justified by the need of reducing the computational cost, exploiting as much as possible the symmetries characterizing the physical phenomenon simulated (pure heat diffusion) and the geometrical configuration. Simulations were run in two steps (Fig. 6):

1. A steady-state calculation to determine the initial conditions prior to melting. The sub-cooling temperature ($T_m - \Delta T_{sub}$) was applied as boundary condition to the exterior of the draining pipe, in the region of the freeze-plug; due to the high conductivity of copper, the minimum temperature in the plugs will be approximately equivalent to this sub-cooling temperature at steady-state. A temperature of 923 K was applied to the cavity top to simulate the mean nominal temperature in the core. All other exterior surfaces were modeled as adiabatic;
2. A time dependent calculation, lasting 2000 s, to simulate conditions after loss of power, including the plug melting. Here, all exterior surfaces were modeled as adiabatic except the cavity top, where a time-dependent temperature boundary condition was imposed. It was derived from the following time-trend of the residual heat in the reactor (Tano Retamales et al., 2018):

$$Q(t) = 6.45908 \cdot 10^6 - 6.9200 \cdot 10^5 \ln(t[s]) \qquad (\mathrm{W/m^3}); \tag{10}$$

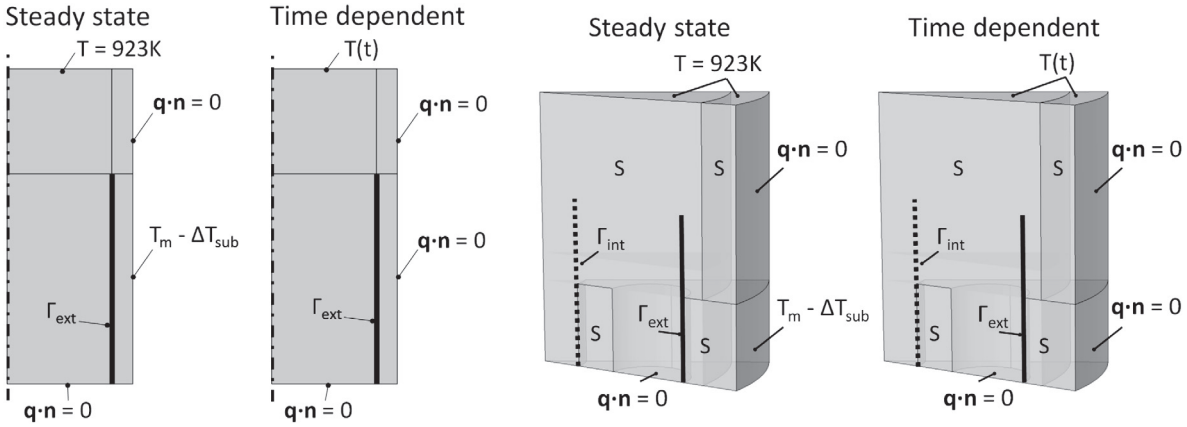

(a) Boundary conditions of the 1-plug design.

(b) Boundary conditions of the 7-plugs design.

Fig. 6. Boundary conditions imposed for the simulations of the 1-plug (left) and the 7-plugs (right) designs. *S* stands for "symmetry" boundary conditions. The plugs edges, external (Γ_{ext}) or internal (Γ_{int}), along which the melting criterion is evaluated are showed with bold lines, solid or dashed, respectively.

by using a lumped capacitance model and assuming no external heat losses, so that

$$Q(t) = \rho c_p \frac{\mathrm{d}T(t)}{\mathrm{d}t}, \tag{11}$$

and applying a polynomial fit to the resulting mean temperature trend, it was found

$$T(t) = -0.0001t^2 + 0.5244t + 923 \quad \text{(K)}. \tag{12}$$

A tetrahedral mesh was used in all simulations, significantly refined in the region of the plug (max element size = 10^{-3} m) in order to ensure a smooth melting front; elsewhere, the default "extremely fine" COMSOL mesh was used. Following the recommendations described in Section 3.1, the phase-change temperature range defining the mushy region was selected to be $\Delta T = 4$ K. Thawing times were computed based on a melting front location in the middle of the mushy region, at $\theta_l = 0.5$. Along an edge Γ, the criterion becomes

$$\int_\Gamma (\theta_l < 0.5)\mathrm{d}s = 0. \tag{13}$$

For the single plug configuration, this criterion was applied to the contact surface with the draining pipe (see Fig. 6a); when it melts completely, the plug is free to fall pushed by the hydrostatic pressure on top of it. In the multi-plug configurations, the melting criterion was applied to all the edges in contact with the copper plate (both internal and external, see Fig. 6b), taking then the maximum melting time. To get more realistic times, these edges had to be extended well above the height of the copper grate, to take into account any frozen layer that could form on top of the plate; in fact, until this layer is completely melted, the plugs in the grate are not free to fall, opening completely the draining pipe.

4. Results

4.1. Steady-state plug shape and frozen salt layer formation on copper grate

Fig. 7 shows cross sections of the steady-state freeze-plug shapes for the two design configurations considered in this work, at recess depths of 0.01 m and 0.10 m and for increasing sub-cooling. For the 7-plug design, both $P/D = 1.05$ and $P/D = 1.50$

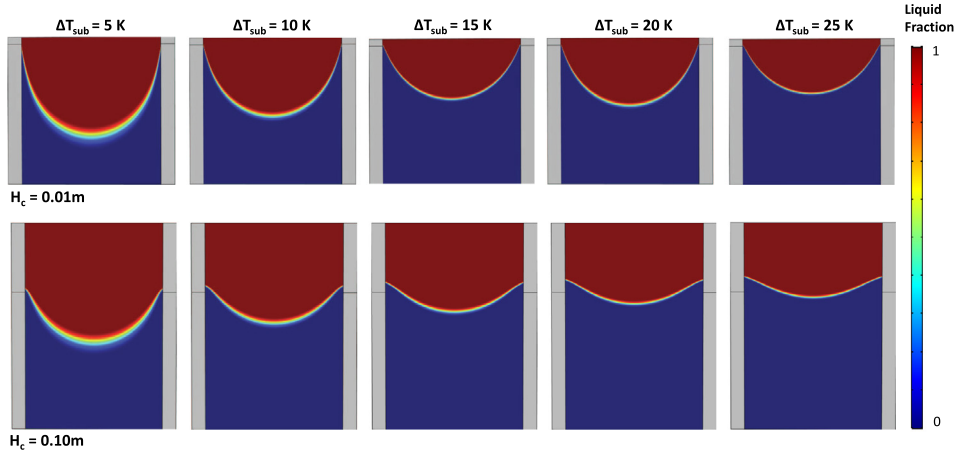

(a) 1-plug design.

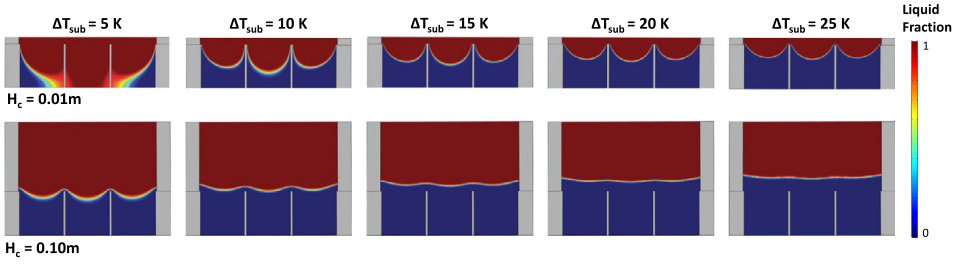

(b) 7-plug design, $P/D = 1.05$.

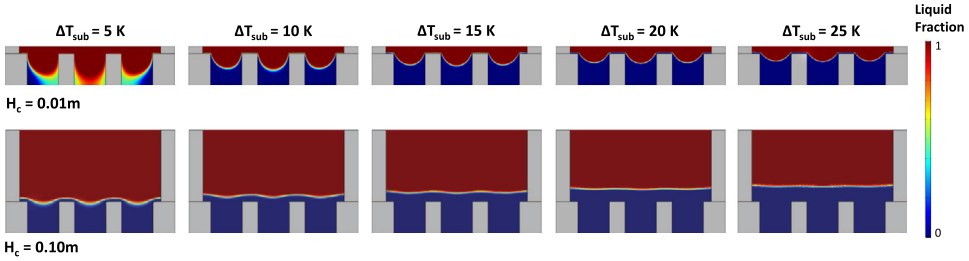

(c) 7-plug design, $P/D = 1.50$.

Fig. 7. Cross sections of steady-state plugs shape (single and multi-plug configurations) for increasing sub-cooling and recess depths.

are shown. At 0.01 m from the core, for all design configurations, the plugs maintain a significant depression in their center for all ΔT_{sub}. Moreover, a sub-cooling of at least 10 K is required to fully form the plug in the 7-plug configuration (for all P/D ratios). On the other hand, at a recess depth of 0.1 m and for all designs, the frozen surface gets less depressed with increasing sub-cooling and, in the 7-plug configuration, is nearly planar for $\Delta T_{sub} > 15$ K. Moreover, for this design, a minimal sub-cooling is required to fully form the plug.

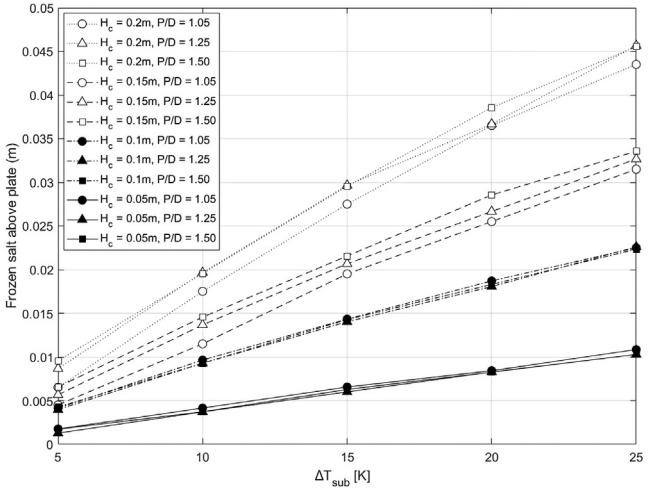

Fig. 8. 7-plug design: Thickness of frozen salt layer above the plate holding the plugs as a function of sub-cooling, recess depth, and P/D ratio.

From Fig. 7, it is clear that, as the 7-plug design is located further away from the core, a frozen salt layer forms on top of the plate, whose thickness depends on ΔT_{sub} as well. A similar phenomenon takes place in the single-plug configuration, where the plug's extension beyond the copper plate increases both with the sub-cooling and the recess depth. Given the influence of the frozen layer on the melting time of the multi-plug design (as explained in the following section), we investigated which factors affect its thickness, and we summarized the findings in Fig. 8. The thickness of the frozen layer on top of the grate increases with the distance of the plug from the core cavity and the sub-cooling. When H_c is 0.01 m, the salt layer is insignificant, while for $H_c = 0.05$ m, the layer thickness increases by approximately 2–2.5 mm per 5 K increase in sub-cooling. For a recess depth of 0.2 m, the growth rate approximately quadruples. At all ΔT_{sub}, the thickness increases roughly linearly with the recess depth, as one would expect from the solution of a simple 1D heat conduction problem across the cavity (taking the copper plate at a uniform temperature of $T_m - \Delta T_{sub}$). The P/D ratio, on the other hand, has a minimal influence on the layer thickness, as Figs. 7b and 7c visually confirm.

4.2. Freeze-plug melting

Fig. 9 summarizes the main results of this study, showing melting times at increasing recess depths, for all P/D ratios and sub-coolings considered. For the 7-plug design, melting times are shown for both the full thickness of the plug, including any salt layer above the copper plate, and only for the portion in contact with the copper plate edge, whose height is equal to H_p (Fig. 3b), to distinguish and underline the effect of the salt layer. The actual melting time for this configuration was taken as the maximum

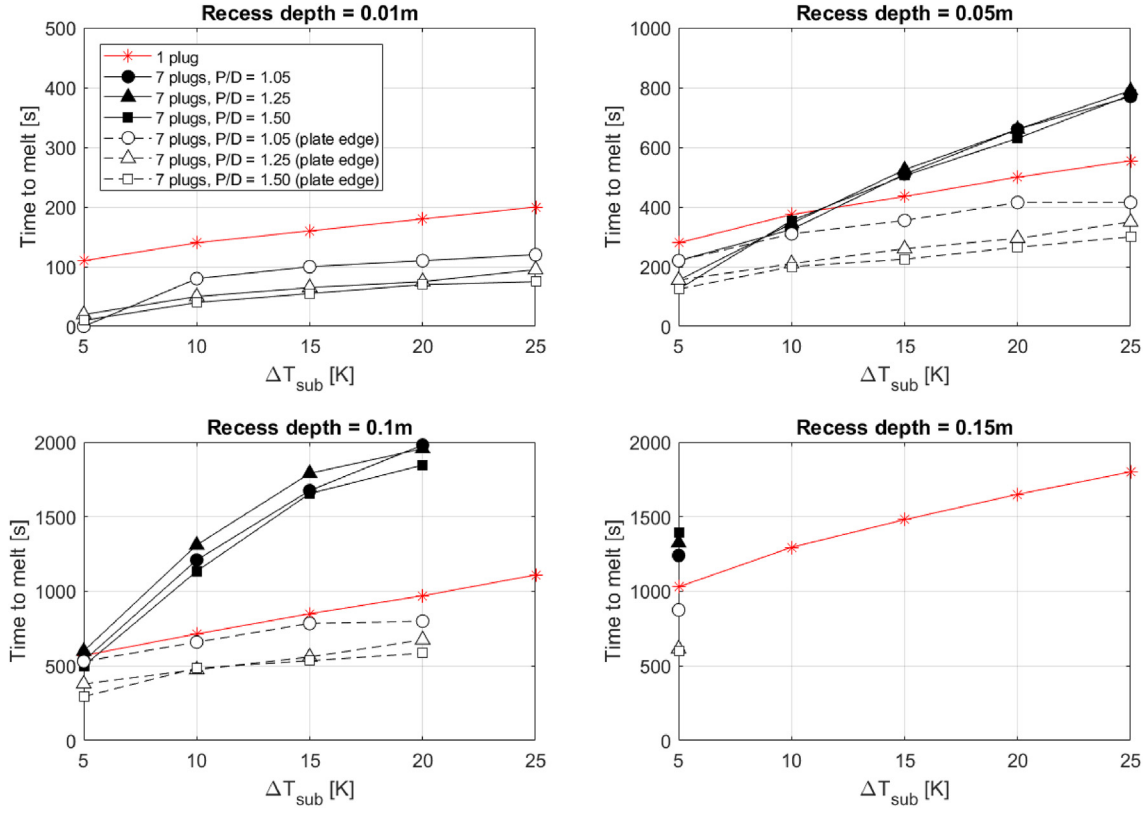

Fig. 9. Melting times as a function of sub-cooling for all P/D ratios and recess depths. For the 7-plug design, melting times are shown for both the full thickness of the plug and only for the portion in contact with the copper plate edge (indicated with "plate edge"), to highlight the effect of the salt layer on top of the plate (the two melting times are equal for a recess depth of 0.01 m because no frozen layer is formed). Limited data are shown for a recess depth of 0.15 m because most models did not melt within the simulation time of 2000 s.

between the two, as explained in Section 3.2, because the plug is not free to fall until it is detached from the pipe walls and the frozen layer on top is completely melted. Detailed numerical results are reported in A. Limited data are shown for a recess depth of 0.15 m because most models did not melt within the simulation time of 2000 s. For the same reason, no data are reported for a recess depth of 0.2 m.

4.2.1. Effect of sub-cooling and recess depth

Fig. 9 shows that the correlation between melting times and sub-cooling becomes stronger with the recess depth. This is due to the fact that, in general, unlike the 1-plug configuration, thawing times for the 7-plug design are driven by the increasing thickness of the frozen layer above the plugs, which increases with both H_c and ΔT_{sub}, as described in Section 4.1.

At a recess depth of 0.01 m, instead, no frozen layer forms, and, consequently, all configurations melt rapidly (within 120 s for the 7-plug design and 200 s for the single-plug) with a weak dependency on the amount of sub-cooling. At $\Delta T_{sub} = 5$ K, for $P/D = 1.05$, no plug forms at all: This explains the null melting time shown in the top left plot of Fig. 9.

Fig. 10 summarizes the melting times at sub-cooling of 5 K and 10 K, for increasing recess depths. Results confirm that the melting speed is controlled by the thickness of the frozen salt layer on top of the plate. In fact, one can clearly see that the melting time of the 7-plug design has approximately a quadratic dependence on H_c (with the frozen layer thickness linearly proportional to it). This follows what one would expect from the solution of a 1D Stefan problem applied to the frozen salt layer (Vuik, 1993).

4.2.2. Effect of P/D ratio

Focusing on the multi-plug configuration, the P/D ratio weakly influences the melting time, compared to the other design parameters. In fact, as shown by Fig. 8, the P/D ratio has a negligible effect on the thickness of the frozen layer on top of the copper plate, which drives the melting process. The three designs considered melted within 20 s of one another when the recess depths is 0.01 m, 10–17 s for $H_c = 0.05$ m, and 50–88 s when $H_c = 0.1$ m. The behavior of the $P/D = 1.05$ is slightly less favorable, though: the edges of this plug melted substantially later than in the other designs. Indeed, while the edges are melting, the plate is still insulated by the frozen layer above it (Fig. 11), so the edges are melted by the heat transferred through the draining pipe and through the sides of the plate; with a P/D ratio of 1.05, however, heat transfer to the middle of the plate is limited by the thin copper walls between the plugs.

4.2.3. Comparison between single and 7-plug designs

At 0.01 m away from the core, the 7-plug design melts faster than the 1-plug design. As the recess depth increases, the 1-plug design becomes increasingly favorable, as the frozen layer on top of the copper grate of the 7-plug design inhibits complete melting.

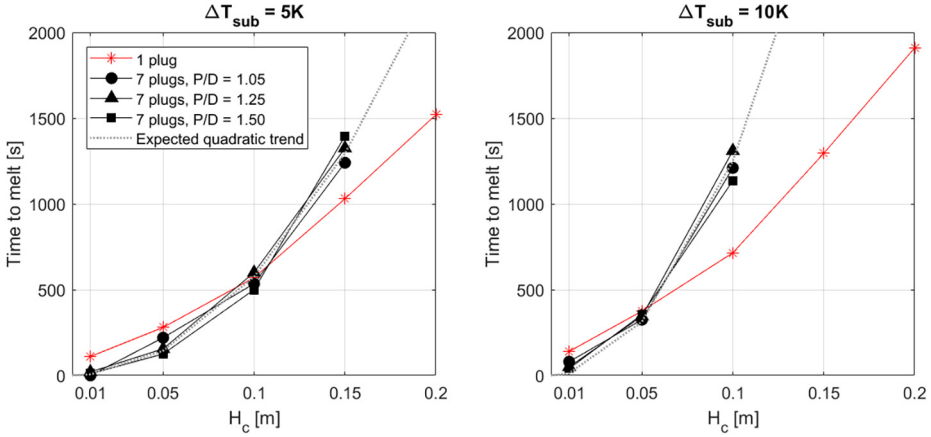

Fig. 10. Melting time as a function of recess depth for 5 K (left) and 10 K (right) of sub-cooling. Melting times for the 7-plug design roughly follow the quadratic trend expected from the solution of a 1D Stefan problem, confirming the process is governed by the thickness of the frozen layer forming on top of the plate.

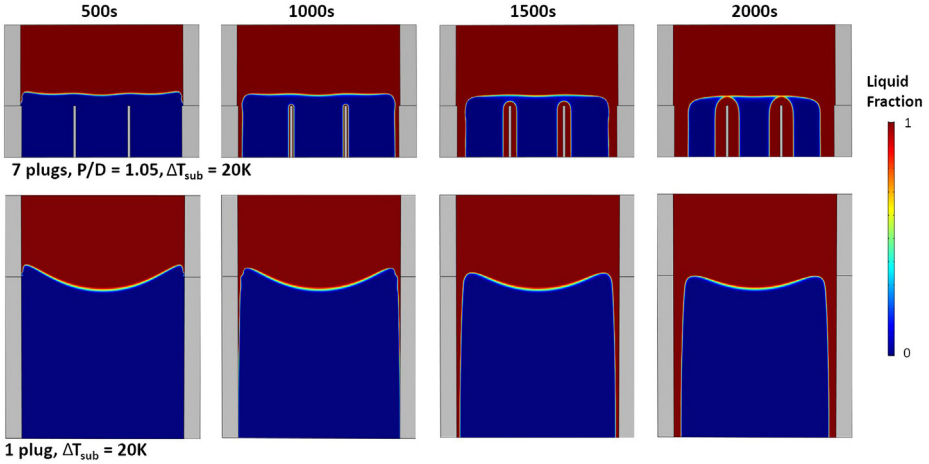

Fig. 11. Cross sections of melting process for 7-plug design with $P/D = 1.05$ (top) and 1-plug design (bottom), with plugs located 0.10 m from the core cavity and with 20 K sub-cooling. The frozen layer on top of the plate considerably delays the complete melting of the multi-plug valve.

When the recess depth is 0.05 m, the single plug has comparable melting times to the 7-plug design at $\Delta T_{sub} \leqslant 10$ K and outperforms it for $\Delta T_{sub} > 10$ K. At $H_c = 0.1$ m, the single plug has a comparable melt time to the 7-plug design for sub-cooling of 5 K and strongly outperforms it at larger ΔT_{sub}. At depths larger than 0.15 m, the single-plug strongly outperforms the 7-plug configurations, most of which did not even melt within 2000 s. One can notice that, as H_c increases, the melting times of the single plug become increasingly comparable to the melting time of the contact edges of the multi-plug designs.

Fig. 11 shows several snapshots of the melting process for plugs located 0.10 m from the core with sub-cooling of 20 K. Here, one can clearly see how the contact edges of the plugs melt long before the frozen layer above the copper plate. Indeed, the layer is melted from the bottom up, by heat conducted through the draining pipe and through the copper plate, rather than by conduction through the molten salt in the pipe, due to the (much) higher conductivities of the Hastelloy-N and copper.

These images highlight, however, that the melting times estimated in this work for the multi-plug design are quite conservative. For example, a layer of molten salt is clearly visible between the copper plate and the remaining part of frozen layer after 1500 s. Realistically, the frozen layer will be continuously pushed against the copper plate by the hydrostatic pressure in the draining pipe and the fluid portion will be squeezed out. This will ensure that the frozen layer is in direct contact with the plate at all times, and will accelerate the melting process. One should assume, therefore, that more realistic melting times lie somewhere between the time required to melt the inside edges of the plugs and the times reported in this study (i.e., between the solid and the dashed lines in Fig. 9). Moreover, when the external edges of the plug are melted (e.g, after 1000 s for the configuration depicted in Fig. 11) the pipe partially opens and the draining of the core salt starts. In this situation, on the one hand, the hypothesis of pure heat conduction is not valid anymore and forced convection will accelerate melting; on the other hand, a partially opened pipe could make longer melting times acceptable. However, only with combined simulations of draining and melting, which we did not carry out in this preliminary study, one can draw definitive conclusions on the acceptability of the multi-plug designs in terms of total melting plus draining time (Wang et al. (2016) show that a partially melted freeze-plug strongly affects draining time).

5. Conclusions

This paper has presented preliminary results on the melting behavior of the freeze-plug, a key safety component of the Molten Salt Fast Reactor. It is a passive valve that should melt fast when the temperature of the salt reaches too high values, thus allowing the drainage of the salt in tanks where it is kept in safe and subcritical conditions. As accident scenario, we considered a power outage followed by reactor shutdown. In fact, this is considered the most severe accident in which the freeze-plug valve has to prove its reliability. The influence on melting time of some design configurations and parameters (plug position along the draining pipe, sub-cooling at nominal condition, P/D ratio, recess depth) has been assessed.

Several conclusions and recommendations for future studies can be drawn:

- A single-plug design is generally favorable over a multi-plug one, especially for distances from the core higher than 0.05 m and for sub-cooling above 5 K. In the multi-plug design, complete melting is inhibited by the presence of a frozen layer on top of the plate. However, further study into the melting behavior of this layer, taking its sinking into account, is required to better quantify the differences in melting time between the two design configurations;
- In a multi-plug configuration, the P/D ratio has a small influence on melting; therefore, its value should derive from the optimization of the draining time;
- Melting times below 1000 s were observed only for recess depths lower than 0.1 m (for all plugs and ΔT_{sub}), and at 0.1 m for $\Delta T_{sub} < 10$ K for the 7-plug design and $\Delta T_{sub} \leqslant 20$ K for the single plug. Therefore, in the absence of a significant mixing in the pipe portion above, the freeze-plug should be located within 0.1 m of the mixed flow to melt quickly enough; and
- In case of a multi-plug configurations, combined simulations of melting and draining should be carried out to derive not too conservative conclusions about the acceptability of a design; in fact, the plug external edges melt way before the frozen layer on top of the plate completely thaws (after which the plug is free to fall). So, longer melting times can be acceptable.

Given the third observation, in spite of the approximations adopted and the limits of the current analysis, we conclude that a freeze-plug design based only on the decay heat to melt is likely to be unfeasible. Indeed, despite the lack of constraints currently set regarding the position of the plug along the draining pipe, it is sensible to say it should be located way more than 0.1 m away from the reactor core, in order to allow room for electrical cooling equipment on the outside of the draining pipe, and to protect the plug from large temperature oscillations (during transient operations) that could cause a premature and unwanted melt. For this reason, within the SAMOFAR project, the design of the freeze-plug valve is currently being improved at LPSC-Grenoble (CNRS, France) laboratories (Giraud et al., 2018). To preserve passivity, melting is enhanced by heat stored in metal structures adjacent to the draining pipe.

Disclaimer

The content of this paper does not reflect the official opinion of the European Union. Responsibility for the information and/or views expressed therein lies entirely with the authors.

Acknowledgments

This project has received funding from the Euratom research and training programme 2014-2018 under grant agreement No 661891.

Appendix A. Melting times

In this Appendix (Tables A.3,A.4,A.5,A.6), we report all results obtained in the melting simulations of the considered freeze-plug designs. Here, H_c indicates the distance of the plug from the core cavity, H_p is the height of the copper plate in contact with the plug (chosen equal to the plug diameter, to maintain an aspect ratio of one), whereas H_{plug} is the maximum effective height the plug assumes on formation; ΔT_{sub} is the maximum sub-cooling; Δt_{melt} is the computed melting time. For the 7-plug design, we report the melting times for both the full thickness of the plug (Δt_{melt}) and only for the portion in contact with the copper plate edge ($\Delta t_{melt,H_p}$). This highlights the effect of the salt layer on top of the plate, whose thickness is indicated with H_l. For $H_c = 0.01$ m, there is no difference between the two melting times because no layer forms on top of the copper plate. Moreover, for $\Delta T_{sub} = 5$ K and $P/D = 1.05$, the melting time is zero. This datum was reported just for completeness and can be explained by the fact that, so close to the core cavity and with such small sub-cooling, no plug forms at

Table A.3
Data 1-plug design.

H_c (m)	0.01					0.05					0.10				
ΔT_{sub} (K)	5	10	15	20	25	5	10	15	20	25	5	10	15	20	25
H_{plug} (m)	0.195	0.200	0.201	0.201	0.202	0.202	0.204	0.207	0.209	0.211	0.205	0.210	0.214	0.219	0.222
Δt_{melt} (s)	110	140	160	180	200	280	375	435	500	555	570	715	850	970	1110

H_c(m)	0.15					0.20				
ΔT_{sub} (K)	5	10	15	20	25	5	10	15	20	25
H_{plug} (m)	0.207	0.215	0.222	0.228	0.234	0.210	0.220	–	–	–
Δt_{melt} (s)	1030	1295	1480	1650	1800	1520	1910	–	–	–

Table A.4
Data 7-plug design for $P/D = 1.05$.

H_c (m)	0.01					0.05					0.10				
ΔT_{sub} (K)	5	10	15	20	25	5	10	15	20	25	5	10	15	20	25
H_p (m)	0.063	0.063	0.063	0.063	0.063	0.063	0.063	0.063	0.063	0.063	0.063	0.063	0.063	0.063	0.063
H_{plug} (m)	0.060	0.064	0.064	0.064	0.065	0.065	0.068	0.070	0.072	0.074	0.068	0.073	0.078	0.082	0.086
H_l (m)	0.000	0.000	0.001	0.001	0.001	0.002	0.004	0.007	0.008	0.011	0.004	0.010	0.014	0.019	0.023
Δt_{melt} (s)	0	80	100	110	120	220	325	510	660	770	535	1210	1675	1980	–
$\Delta t_{melt,H_p}$ (s)	0	80	100	110	120	220	310	355	415	415	530	660	785	800	–

H_c (m)	0.15					0.20				
ΔT_{sub} (K)	5	10	15	20	25	5	10	15	20	25
H_p (m)	0.063	0.063	0.063	0.063	0.063	0.063	0.063	0.063	0.063	0.063
H_{plug} (m)	0.068	0.075	0.083	0.089	0.095	0.070	0.081	0.091	0.100	0.107
H_l (m)	0.005	0.012	0.019	0.025	0.031	0.007	0.017	0.027	0.037	0.044
Δt_{melt} (s)	1240	–	–	–	–	–	–	–	–	–
$\Delta t_{melt,H_p}$ (s)	875	–	–	–	–	–	–	–	–	–

Table A.5
Data 7-plug design $P/D = 1.25$.

H_c (m)	0.01					0.05					0.10				
ΔT_{sub} (K)	5	10	15	20	25	5	10	15	20	25	5	10	15	20	25
H_p (m)	0.053	0.053	0.053	0.053	0.053	0.053	0.053	0.053	0.053	0.053	0.053	0.053	0.053	0.053	0.053
H_{plug} (m)	0.053	0.053	0.054	0.054	0.055	0.055	0.057	0.059	0.062	0.064	0.057	0.063	0.067	0.071	0.076
H_l (m)	0.000	0.000	0.001	0.001	0.001	0.001	0.004	0.006	0.008	0.010	0.004	0.009	0.014	0.018	0.023
Δt_{melt} (s)	20	50	65	75	95	155	345	525	660	790	600	1310	1790	1955	–
$\Delta t_{melt,H_p}$ (s)	20	50	65	75	95	155	210	260	295	350	380	475	560	675	–

H_c (m)	0.15					0.20				
ΔT_{sub} (K)	5	10	15	20	25	5	10	15	20	25
H_p (m)	0.053	0.053	0.053	0.053	0.053	0.053	0.053	0.053	0.053	0.053
H_{plug} (m)	0.059	0.067	0.074	0.080	0.086	0.062	0.073	0.083	0.090	0.099
H_l (m)	0.006	0.014	0.021	0.027	0.033	0.009	0.019	0.029	0.037	0.045
Δt_{melt} (s)	1325	–	–	–	–	–	–	–	–	–
$\Delta t_{melt,H_p}$ (s)	615	–	–	–	–	–	–	–	–	–

Table A.6
Data 7-plug design for $P/D = 1.50$.

H_c (m)	0.01					0.05					0.10				
ΔT_{sub} (K)	5	10	15	20	25	5	10	15	20	25	5	10	15	20	25
H_p (m)	0.044	0.044	0.044	0.044	0.044	0.044	0.044	0.044	0.044	0.044	0.044	0.044	0.044	0.044	0.044
H_{plug} (m)	0.044	0.045	0.045	0.045	0.046	0.046	0.048	0.051	0.053	0.055	0.049	0.054	0.059	0.063	0.067
H_l (m)	0.000	0.000	0.001	0.001	0.001	0.002	0.004	0.006	0.008	0.010	0.004	0.009	0.014	0.018	0.022
Δt_{melt} (s)	10	40	55	70	75	125	355	505	630	775	500	1135	1655	1845	–
$\Delta t_{melt,H_p}$ (s)	10	40	55	70	75	125	200	225	265	300	295	485	535	585	–

H_c (m)	0.15					0.20				
ΔT_{sub} (K)	5	10	15	20	25	5	10	15	20	25
H_p (m)	0.044	0.044	0.044	0.044	0.044	0.044	0.044	0.044	0.044	0.044
H_{plug} (m)	0.051	0.059	0.066	0.073	0.078	0.054	0.064	0.074	0.083	0.090
H_l (m)	0.007	0.014	0.022	0.028	0.033	0.010	0.020	0.029	0.038	0.046
Δt_{melt} (s)	1395	–	–	–	–	–	–	–	–	–
$\Delta t_{melt,H_p}$ (s)	598	–	–	–	–	–	–	–	–	–

steady state. A "–" means that the melting time is not available since the model did not melt within the simulation time of 2000 s.

References

Aji, I.K., Kinoshita, M., Tatsuya, T., Okawa, T., 2018. An experimental study on freeze valve performance in a molten salt reactor. ICONE-26: The 26th International Conference on Nuclear Engineering, vol. 9. London, England.

Alexiades, V., Solomon, A.D., 1993. Mathematical Modeling of Melting and Freezing Processes. Hemisphere Publishing.

Allibert, M., Aufiero, M., Brovchenko, M., Delpech, S., Ghetta, V., Heuer, D., Laureau, A., Merle-Lucotte, E., 2016. Molten salt fast reactors. In: Pioro, I.L. (Ed.), Handbook of Generation IV Nuclear Reactors. Woodhead Publishing, pp. 157–188.

Beneš, O., Konings, R.J.M., 2009. Thermodynamic properties and phase diagrams of fluoride salts for nuclear applications. J. Fluorine Chem. 130, 22–29.

Brovchenko, M., Heuer, D., Merle-Lucotte, E., Allibert, M., Ghetta, V., Laureau, A., Rubiolo, P., 2013. Design-related studies for the preliminary safety assessment of the molten salt fast reactor. Nucl. Sci. Eng. 175, 329–339.

Capelli, E., Beneš, O., Beilmann, M., Konings, R.J.M., 2013. Thermodynamic investigation of the LiF-ThF4 ystem. J. Chem. Thermodynamicsy 58, 110–116.

COMSOL Multiphysics®, 2017. Reference Manual Version 5.3. Stockholm, Sweden.

Friedman, E., 2005. Circles in Circles on Erich's Packing Center. URL:https://www2.stetson.edu/efriedma/cirincir/ (accessed 01.10.2019).

Generation IV International Forum, 2002. A Technology Roadmap for Generation IV Nuclear Energy Systems. Technical Report GIF-002-00 U.S. DOE Nuclear Energy Research Advisory Committee and the Generation IV International Forum.

Gérardin, D., Allibert, M., Heuer, D., Laureau, A., Merle-Lucotte, E., Seuvre, C., 2017. Design evolutions of Molten Salt Fast Reactor. In: International Conference on Fast Reactors and Related Fuel Cycles: Next Generation Nuclear Systemes for Sustainable Development (FR17). Yekaterinburg, Russia.

Giraud, J., Ghetta, V., Rubiolo, P., Tano Retamales, M., 2018. Development and test of a cold plug valve with fluoride salt. In: 12th International Topical Meeting on Nuclear Reactor Thermal-Hydraulics, Operation and Safety (NUTHOS-12). Qingdao, China.

Graham, R.L., 1968. Sets of points with given minimum separation (Solution to Problem E1921). Am. Math. Month. 75, 192–193.

Haubenreich, P.N., Engel, J.R., 1970. Experience with the Molten-Salt Reactor Experiment. Nucl. Appl. Technol. 8, 118–136.

Heuer, D., Merle-Lucotte, E., Allibert, M., Brovchenko, M., Ghetta, V., Rubiolo, P., 2014. Towards the thorium fuel cycle with molten salt fast reactors. Ann. Nucl. Energy 64, 421–429.

Iwatsu, R., Hyun, J., Kuwahara, K., 1993. Mixed convection in a driven cavity with a stable vertical temperature gradient. Int. J. Heat Mass Transfer 36, 1601–1608.

Jiang, M.H., Xu, H.J., Dai, Z.M., 2012. Advanced fission energy program-TMSR nuclear energy system. Bull. Chin. Acad. Sci. 27, 366–374.

Jin, X., Hu, H., Shi, X., Zhou, X., Zhang, X., 2018. Comparison of two numerical heat transfer models for phase change material board. Appl. Therm. Eng. 128, 1331–1339.

Koger, J.W., 1972. Evaluation of Hastelloy N alloys after nine years exposure to both a molten fluoride salt and air at temperatures from 700 to 560°C (Report ORNL-TM-4189). Oak Ridge National Laboratory.

Kong, X., Fu, Y., Zhang, J., Lu, H., Wang, N., 2018. Upgrade and shakedown test of a high temperature fluoride salt test loop. The 26th International Conference on Nuclear Engineering, 9. London, England.

LeBlanc, D., 2010. Molten salt reactors: a new beginning for an old idea. Nucl. Eng. Des. 240, 1644–1656.

MacPherson, H.G., 1985. The Molten Salt reactor adventure. Nucl. Sci. Eng. 90, 374–380.

Makkinje, A., 2017. Design of a freeze plug grate (Bachelor's thesis). TU Delft.

Nikrityuk, P.A., 2011. Computational thermo-fluid dynamics. In: Materials Science and Engineering. Wiley-VCH Verlag GmbH & Co. KGaA.

Richardson, M., 1962. Development of Freeze Valve for use in the MSRE (Report ORNL-TM-128). Oak Ridge National Laboratory.

Robertson, R.C., 1965. MSRE Design and operation report – Part I (Report ORNL-TM-728). Oak Ridge National Laboratory.

Rubiolo, P., Tano Retamales, M., Ghetta, V., Giraud, J., 2017. High temperature thermal hydraulics modeling of a molten salt: application to a molten salt fast reactor (MSFR). ESAIM Proc. Surveys 58, 98–117.

Rubiolo, P., Tano Retamales, M., Giraud, J., Ghetta, V., Blanco, J., Doche, O., Capellan, N., 2018. Design of close and open channel experiments to study molten salt flows. Proceedings of the 2018 International Congress on Advances in Nuclear Power Plants, ICAPP 2018, vol. 115, pp. 397–405. Charlotte, North Carolina.

Serp, J., Allibert, M., Beneš, O., Delpech, S., Feynberg, O., Ghetta, V., Heuer, D., Holcomb, D., Ignatiev, V., Kloosterman, J.L., Luzzi, L., Merle-Lucotte, E., Uhlíř, J., Yoshioka, R., Zhimin, D., 2014. The molten salt reactor (MSR) in generation IV: overview and perspectives. Prog. Nucl. Energy 77, 308–319.

Swaminathan, C.R., Voller, V.R., 1993. On the enthalpy method. Int. J. Numer. Methods Heat Fluid Flow 3, 233–244.

Tano Retamales, M., Rubiolo, P., Doche, O., 2017. Progress in modeling solidification in molten salt coolants. Modell. Simul. Mater. Sci. Eng. 2017, 98–117.

Tano Retamales, M., Rubiolo, P., Giraud, J., Ghetta, V., 2018. Multiphysics study of the draining transients in the Molten Salt Fast Reactor. Proceedings of the 2018 International Congress on Advances in Nuclear Power Plants, ICAPP 2018, vol. 115, pp. 469–478. Charlotte, North Carolina.

Van Tuyll, F., 2016. A new design for the safety plug in a Molten Salt Fast Reactor (Bachelor's thesis). TU Delft.

Voller, V., Cross, M., 1981. Accurate solutions of moving boundary problems using the enthalpy method. Int. J. Heat Mass Transfer 24, 545–556.

Voller, V.R., Swaminathan, C.R., Thomas, B.G., 1990. Fixed grid techniques for phase change problems: a review. Int. J. Numer. Meth. Eng. 30, 875–898.

Vuik, C., 1993. Some historical notes on the Stefan problem. Nieuw Archief voor Wiskunde 11, 157–167.

Wang, S., Massone, M., Rineiski, A., Merle-Lucotte, E., 2016. Analytical investigation of the draining system for a Molten Salt Fast Reactor. In: NUTHOS- 11: The 11th International Topical Meeting on Nuclear Reactor Thermal Hydraulics, Operation and Safety. Gyeongju, Korea.